Oil & Gas Science and Technology – Rev. IFP Energies nouvelles, Vol. 66 (2011), No. 2, pp. 181-191

DOI: 10.2516/ogst/2010023

IFP Energies nouvelles International Conference
Rencontres Scientifiques d'IFP Energies nouvelles

Chemical Looping - An Alternative Concept for Efficient and Clean Use of Fossil Resources
La Boucle Chimique - Un concept alternatif pour un usage propre et efficace des ressources fossiles

Chemical Looping Combustion of Solid Fuels in a 10 kW_{th} Unit

N. Berguerand*, A. Lyngfelt, T. Mattisson and P. Markström

Chalmers University of Technology, 412 96 Göteborg - Sweden
email: nicoberg@chalmers.se - anders.lyngfelt@chalmers.se - tm@chalmers.se - pontus.markstrom@chalmers.se

* Corresponding author

Résumé — Combustion de charge solide en boucle chimique dans une unité de 10 kW_{th} — Cette étude est basée sur des résultats antérieurs obtenus dans une unité de combustion de charges solides en boucle chimique d'une puissance de 10 kW_{th}. Le transporteur d'oxygène utilisé est de l'ilménite, un minerai de fer et de titane, et les charges solides étudiées sont, d'une part, un coke de pétrole mexicain et, d'autre part, un charbon bitumineux sud africain. Les résultats expérimentaux ont été obtenus à des températures allant jusqu'à 1030°C avec différents débits de transporteur d'oxygène entre les réacteurs d'oxydation et de réduction. La modélisation de la combustion en boucle chimique de charges solides a déjà permis d'établir une corrélation entre le débit de circulation de transporteur d'oxygène et les données expérimentales mesurées puis de modéliser le taux de captage en fonction du temps de séjour du charbon et de sa réactivité. La cinétique de conversion du charbon a de plus été établie et permet de représenter les résultats expérimentaux de manière satisfaisante. Cette étude vise à compléter la modélisation entreprise pour prédire la conversion du gaz de synthèse résultant de la gazéification du charbon au contact de l'ilménite, en s'appuyant sur des données obtenues par ATG et dans un lit fluidisé en batch. Les résultats obtenus par modélisation sont comparés aux conversions mesurées expérimentalement dans l'unité de 10 kW_{th}.

Abstract* — *Chemical Looping Combustion of Solid Fuels in a 10 kW_{th} Unit — *The present study is based on previous results from batch experiments which were conducted in a 10 kW_{th} chemical looping combustor for solid fuels using ilmenite, an iron titanium oxide, as the oxygen carrier with two solid fuels: a Mexican petroleum coke and a South African bituminous coal. These experiments involved testing at different fuel reactor temperatures, up to 1030°C, and different particle circulation rates between the air and fuel reactors. Previous results enabled modeling of the reactor system. In particular, it was possible to derive a correlation between measured operational data and actual circulation mass flow, as well as a model that describes the carbon capture efficiency as a function of the residence time and the char reactivity. Moreover, the kinetics of char conversion could be modeled and results showed good agreement with experimental values. The purpose of the present study was to complete these results by developing a model to predict the conversion of syngas with ilmenite in the fuel reactor. Here, kinetic data from investigations of ilmenite in TGA and batch fluidized bed reactors were used. Results were compared with the actual conversions during operation in this 10 kW_{th} unit.*

ACRONYMS AND NOTATIONS

AR/FR	Air/Fuel Reactor
CS	Carbon Stripper
FRPL	Fuel reactor loop-seal
HIVEL	High velocity section
LOVEL	Low velocity section
PSD	Particle Size Distribution
b	Stoichiometric coefficient ($mol_{ilmenite}/mol_{fuel}$)
CI	Circulation Index (kPa·L/min)
C	Molar concentration of reactant (mol/m^3)
E	Activation energy (kJ/mol)
F_0	Fluidizing flow at the bed bottom (Nm^3/min)
F_m	Fluidizing flow at a level corresponding to a mass "m" in the bed (Nm^3/min)
F_g	Flow of syngas released from the char (Nm^3/min)
f_{OF}	Stoichiometric ratio of oxygen consumed per mol of fuel oxidized
k	Initial reaction rate constant, species related ($mol^{1-n}.m^{3n-2}/s$)
k_{eff}	Mass-based reaction rate constant, species related (1/s)
k_F	Mass-based and flow-normalized reaction rate constant, species related ($Nm^3/(ton.s)$)
M_O	Molecular weight of oxygen (16 kg/kmol)
m_{tot} or m	Oxygen carrier inventory (kg or ton)
m_{ox}/m_{red}	Mass of a fully oxidized/reduced oxygen carrier particle (g)
$\dot{m}$	Particle circulation (kg/min)
N	Number of beds in series in CSTR modeling
n	Reaction order
p	Partial pressure of reactant (bar)
p_0	Inlet partial pressure of reactant (bar)
p_1	Outlet partial pressure reactant (bar)
p_g	Partial pressure of reactant originating from char gasification (bar)
p_m	Mean partial pressure of reactant in the bed (bar)
p_{tot}	Total pressure (*i.e.* 1 bar)
r_g	Grain radius (m)
R	Ideal gas constant (8.314 J/(mol.K))
R_0	Theoretical oxygen-transfer capacity of the oxygen carrier (%)
T	Temperature (°C)
t	Time (min or s)
V_n	Normal molar volume (22.4 $Nm^3/kmol$)
X	Degree of conversion of oxygen carrier (%)
α	Dimensionless number
γ	Conversion of reactant (%)
γ_A	Conversion of reactant in method A (%)
η_{CC}	Carbon capture efficiency (%)
κ	Dimensionless number
ω	Degree of mass-based conversion (%)
Ω_{OD}	Oxygen demand (-) or (%)
ρ_m	Molar density of active solid phase (mol/m^3)
τ	Residence time in fuel reactor system (min)
τ_{comp}	Time to reach complete conversion of an oxygen carrier particle (s)

INTRODUCTION

Chemical Looping Combustion (CLC) is a novel fuel conversion technology with inherent CO_2 capture. In the CLC process, the oxygen is directly transferred to the fuel via a circulating oxygen carrier in the form of a metal oxide, avoiding the presence of nitrogen in the exhaust flue gas, see Figure 1.

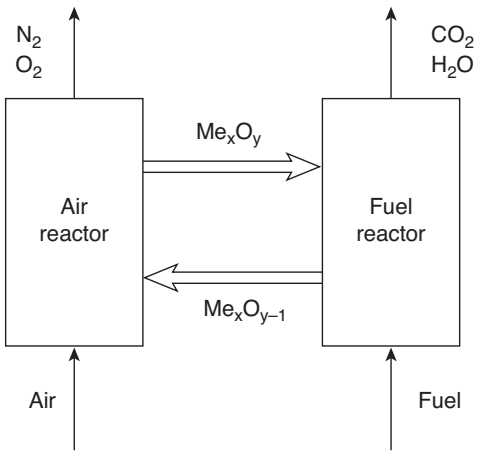

Figure 1

The Chemical Looping Combustion principle.

The oxidation of the oxygen carrier takes place in a so-called Air Reactor (AR) while it is reduced in the Fuel Reactor (FR). Denoting Me_xO_y and Me_xO_{y-1} as the oxidized and reduced form of the oxygen carrier, the general reaction between the fuel and the metal oxide reads:

$$(2n+m)\,Me_xO_y + C_nH_{2m} \rightarrow (2n+m)\,Me_xO_{y-1} + mH_2O + nCO_2 \quad (1)$$

while the oxygen carrier oxidation in the air reactor is:

$$Me_xO_{y-1} + \frac{1}{2}O_2 \rightarrow Me_xO_y \quad (2)$$

In the fuel reactor, CO_2 and H_2O are produced but these are never mixed with the nitrogen in the air as is the case during normal combustion with air. By condensing the steam, almost pure CO_2 can be obtained, which can later be transported to appropriate storage locations. At the outlet of the air reactor, the flue gas contains nitrogen and some unused oxygen. Thus, CO_2 is obtained avoiding active gas separation, as well as costs and energy penalties associated with gas separation.

Depending on the fuel and the oxygen carrier, reaction (1) is often endothermic while reaction (2) is exothermic. The total amount of heat resulting from reactions (1) and (2) is the same as for a normal combustion where the fuel is in direct contact with the air oxygen.

In CLC of solid fuels, the volatile compounds released from the fresh fuel can react according to reaction (1). However, the remaining char needs to be gasified in the fuel reactor using steam or CO_2 according to Equation (3):

$$C + H_2O / CO_2 \rightarrow CO + H_2 / CO \quad (3)$$

The synthesis gases H_2 and CO can then react with the oxygen carrier according to:

$$CO / H_2 + Me_xO_y \rightarrow CO_2 / H_2O + Me_xO_{y-1} \quad (4)$$

Solid fuel CLC has been studied in laboratory units using different types of fuels and oxygen carriers [1-14]. In particular, tests were conducted by Berguerand and Lyngfelt [15-19] and Markström *et al*. [20] in a 10 kW$_{th}$ unit at Chalmers University, totalizing almost 100 h of operation. The oxygen carrier used during these tests was ilmenite, an iron titanium oxide and the fuels a South African bituminous coal and a Mexican petroleum coke. More recently, two other pilots of 1 and 10 kW$_{th}$ were built and operated by Shen *et al*. [21] and Wu *et al*. [22] in China.

This work is based on results from batchwise introduction of fuel into the fuel reactor which gave the possibility to obtain complementary information compared to previous continuous tests. In recent work involving batch tests in this unit, direct evaluation of the oxygen demand associated with the syngas could be achieved. Moreover, the kinetics of char conversion in the fuel reactor was modeled as well as the loss of carbon to the air reactor as a function of the particle circulation. Here the main focus is made on modeling the conversion of syngas produced by char gasification.

1 EXPERIMENTAL BASIS

1.1 The 10 kW$_{th}$ Unit

A detailed description of the 10 kW$_{th}$ unit is provided in references [15, 16]. In this previous work, the fuel feed was continuous and here, the unit is generally operated in the same way except that the fuel is fed in batches. Figure 2 shows a general view over the whole reactor system: air and fuel reactors, particle filters, fuel feeding system, steam generator and water seal.

A schematic view of the different fuel reactor chambers and their dimensions is presented in Figures 3 and 4. Note that the arrows represent the directions of particle circulation. In particular, the fuel reactor is divided in three main chambers:

- the low velocity section (LOVEL) subdivided into two chambers where the fuel is gasified and subsequently oxidized by the oxygen carrier;
- the high velocity section (HIVEL) located below the riser through which both types of particles – but especially the unburnt char – are elutriated; the corresponding amounts depending on the operation/ fluidizing velocity. The reactor system has an internal recirculation loop via a smaller cyclone in order to increase the overall residence time of char particles. However, in the present work, the HIVEL chamber was fluidized at similar velocities as LOVEL;
- the Carbon Stripper (CS) which has the purpose of separating char from oxygen carrier. The unreacted char is recirculated to the low velocity section while the oxygen carrier proceeds to the air reactor for regeneration.

Moreover, two particle loop-seals separate the air and the fuel reactors, accommodating for the pressure differences between the reactors but also preventing cross-contamination of their effluents, see Figure 2. A third loop-seal, called "fuel reactor loop-seals" or FRPL, is located in the internal loop, between the leg of the small fuel reactor cyclone and the freeboard of the low velocity part LOVEL.

1.2 Oxygen Carrier and Solid Fuels

The oxygen carrier used in this work is an iron titanium oxide called ilmenite, which is extracted from a natural ore containing 40%wt ilmenite. It is provided by the Norwegian company Titania A/S and received in its reduced form $FeTiO_3$. The iron/titanium molar ratio in this material is close to 1:1. The material used in the experiment has a pureness of 94.3% and a bulk density measured to 2100 kg/m^3 for the fresh ilmenite. However, studies indicate that the density of ilmenite decreases when the particles are subject to a CLC environment [23].

Oxygen carrier particles introduced into the reactor system were composed mainly of particles between 90 and 250 μm in diameter. The Particle Size Distribution (PSD) is shown in Table 1 below.

Note that ilmenite in this work refers to activated particles as these have previously been used during CLC operation in this unit and thus been subject to numerous consecutive redox cycles. Activation of ilmenite is detailed in [24].

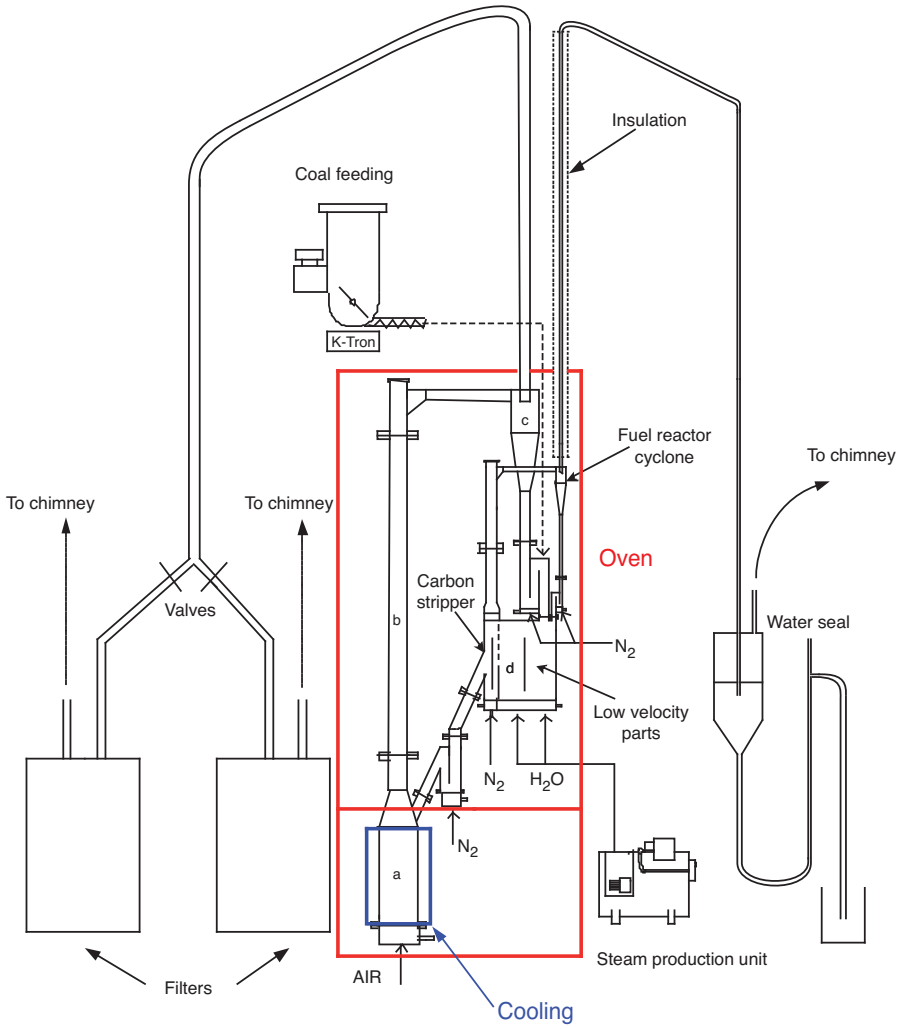

Figure 2

View of the 10 kW_{th} unit: a) air reactor; b) air reactor riser; c) air reactor cyclone; d) fuel reactor.

TABLE 1

Particle size distribution of the ilmenite oxygen carrier (μm)

Diameter Ø (μm)	% (wt)
Ø > 250	7.41
180 < Ø < 250	44.97
125 < Ø < 180	38.10
90 < Ø < 125	8.73
90 < Ø	0.79

In this work, results from two solid fuels are compared: a bituminous coal from the Republic of South Africa (RSA), and a petroleum coke from Mexico. The fuel analysis, for fuels as received, are shown in Table 2.

TABLE 2

Analysis of the solid fuels, as received

Fuel	RSA Coal	Pet coke II
C (%wt)	62.5	84.93
H (%wt)	3.5	3.41
N (%wt)	1.4	1.66
S (%wt)	0.7	6.59
O (%wt)	7.7	0.49
Volatiles (%wt)	21.6	9.91
Ash (%wt)	15.9	1.83
Moisture (%wt)	8.3	1.09
Lower heating value (MJ/kg)	23.9	32.96

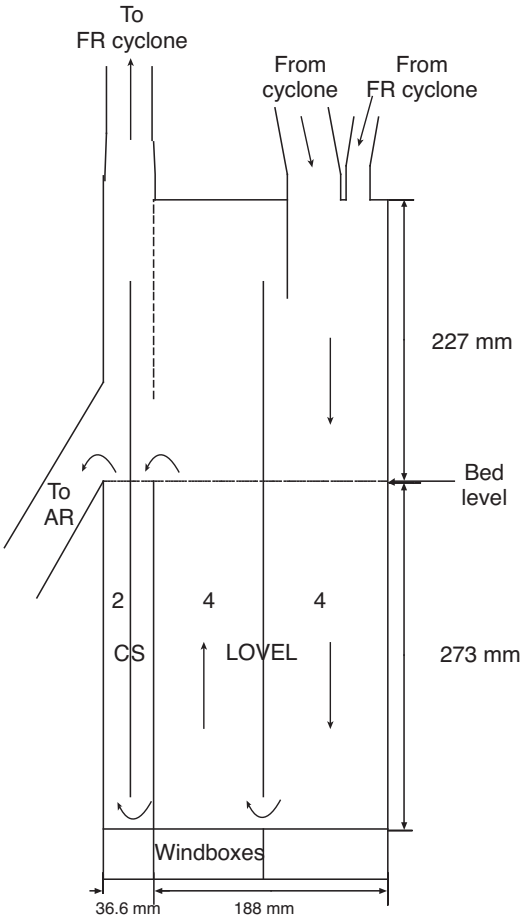

Figure 3

Front view of the fuel reactor chambers (HIVEL is located right behind CS). 2) is the carbon stripper and 4) is the low velocity part LOVEL, divided into two chambers. The direction for the particle circulation are indicated.

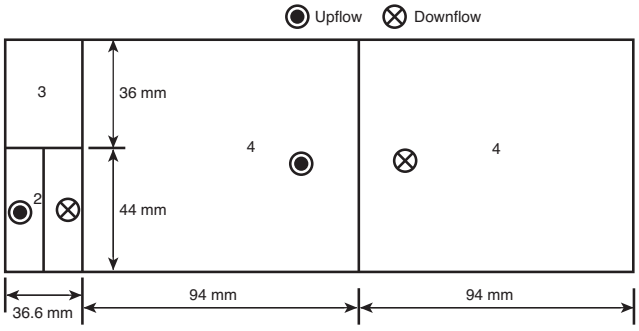

Figure 4

Top view of the fuel reactor. 2) is the carbon stripper CS, 3) is the high velocity part HIVEL and 4) is the low velocity part LOVEL, divided into two chambers. The directions for the particle circulation are indicated.

2 DATA EVALUATION AND PREVIOUS RESULTS

2.1 Data Evaluation

Criteria to assess the performance of operation in the 10 kW$_{th}$ unit need to be introduced. They include:

– the oxygen demand, noted Ω_{OD}, is an indicator of the degree of gas conversion in the fuel reactor and is defined as the fraction of oxygen lacking to achieve complete combustion of the gas produced in the fuel reactor. It depends on the contact and reactivity between the oxygen carrier and the reducing gases and is based on CH_4, CO, H_2 and H_2S;

– the carbon capture efficiency η_{CC}, which is defined as the ratio of gaseous carbon leaving the fuel reactor to the carbon containing gases leaving the system, *i.e.* air and fuel reactors. It reflects the residence time of particles in the fuel reactor and the separation efficiency in the carbon stripper;

– the instantaneous rate of fuel conversion, based on the remaining amount of fuel in the bed at each time step of the reduction period. It is strongly temperature dependent.

2.2 Previous Results from Batch Operation

Results from batch operation in the 10 kW$_{th}$ unit are described in two earlier publications [19, 20]. In particular:

– it can be shown in reference [19] that around 75% of the total oxygen missing for the conversion was associated with the fuel volatiles, confirming earlier estimation [18]. Indeed, due to the fuel feed system with devolatilization occurring above the fuel reactor bed, the volatiles cannot be converted by the oxygen carrier particles. This means that the high oxygen demands usually obtained in testing with continuous feed in this unit are more a consequence of the reactor design than a problem inherent to the process [15-18];

– after batch introduction of fuel in FR and in presence of a particle circulation, the response in AR is displayed by a decrease in the oxygen concentration in the gas leaving AR. The shape of this oxygen consumption curve directly reflects the residence time distribution of the particles in FR. Then, using a model with N multistage well-mixed beds in series, it was possible to determine the residence time and residence time distribution of the particles in FR, for a number of operational cases with different particle circulation. Knowing the solids inventory in the fuel reactor, the actual circulation mass flow could also be determined [20]. Moreover, the circulation mass flow could independently be correlated to measured operational data, *i.e.* pressure drop, temperature and gas flow in AR riser. This correlation could be used to determine the circulation mass flow in previous continuous testing [20];

– using results for CO_2 capture efficiency in the 10 kW_{th} unit and the parameters for the residence time distribution in FR above, a model was developed which could determine a mass-based reaction constant for char conversion. This mass-based reaction constant could also be determined independently from the conversion rates of char during the batch tests. There was good agreement between these two ways of assessing the rate constant, indicating that the model well describes the behavior of the unit. In other words, the model allows the prediction of the CO_2 capture from the particle circulation and char reactivity [20].

Here the idea is to complement these results by developing a model predicting the conversion of syngas in the fuel reactor for comparison with experimental results, using previous data on batch testing in the 10 kW_{th} unit [19, 20].

3 MODELING OF THE SYNGAS CONVERSION

Let us consider a bed of oxygen carrier particles with a total mass m_{tot} and having an even distribution of char particles. When in contact with steam, the char particles will gasify to CO and H_2. These syngases will further react with the oxygen carrier to form CO_2 and H_2O. As the gas produced by gasification is assumed to be released proportionally to the mass, the gas flow F_m at a level of the bed corresponding to a total mass m will be:

$$F_m = F_0\left(1+\kappa\frac{m}{m_{tot}}\right) \tag{5}$$

F_0 is the gas entering at the bottom, *e.g.* fluidizing gas, and κ is defined as:

$$\kappa = \frac{F_g}{F_0} \tag{6}$$

where F_g is the gas released from char gasification. Thus, $\kappa = 0$ would mean that there is no gasification occurring within the bed. Note that the gas flows are normalized to 0°C and 1 bar.

k_F is introduced as a mass-based and volume-normalized rate constant indicating the reactivity, *i.e.* quantifying the ability of the ilmenite to convert the syngas at a certain fuel reactor temperature. Then, from a mass balance over a layer dm of the bed, the difference in partial pressure dp of the reactant, *e.g.* either of the two syngas species formed CO and H_2, can be written as:

$$dp = \left[\frac{-k_F m_{tot}}{F_0}p - \kappa p + p_g\left(1+\kappa\right)\right]\frac{dm}{m_{tot}\left(1+\kappa\cdot m/m_{tot}\right)} \tag{7}$$

In Equation (7), the first term reflects the consumption of syngas reactant (CO or H_2) by reaction, the second the dilution by the release of syngas itself and the third the addition of reactant by syngas release, *i.e.* p_g corresponds to the source of reactant through char gasification. Note that the derivation above is also valid for gaseous fuel, which corresponds to the case $\kappa = 0$ and $p_g = 0$. Equation (7) assumes, in particular, a first order reaction for the consumption of reactant by the oxygen carrier and thus the following discussion is valid for the case of first order reactions. Integrating Equation (7) provides the general solution in Equation (8):

$$p = \frac{1}{\alpha+\kappa}\left\{p_g(1+\kappa)+\left[\left(\alpha+\kappa\right)p_0 - p_g(1+\kappa)\right]\cdot\left(1+\kappa\frac{m}{m_{tot}}\right)^{\frac{\partial}{\kappa}-1}\right\} \tag{8}$$

Here, p_0 is the partial pressure of reactant at the bottom of the bed and α a dimensionless number introduced as:

$$\alpha = \frac{k_F m}{F_0} \tag{9}$$

In the 10 kW_{th} unit, the bed is fluidized with steam, which means that $p_0 = 0$ and at the top of the bed, the partial pressure p in Equation (8) can be written:

$$p = \frac{p_g}{\alpha+\kappa}\left\{(1+\kappa)-\left(1+\kappa\right)^{-\frac{\partial}{\kappa}}\right\} \tag{10}$$

Finally, the conversion of reactant at the top of the bed is derived from Equation (10) to:

$$\gamma = 1-\frac{\left[(1+\kappa)-(1+\kappa)^{-\partial/\kappa}\right]}{\alpha+\kappa} \tag{11}$$

During operation in the 10 kW_{th} unit, the fluidizing flow of steam F_0 is constant at $3\cdot10^{-2}$ Nm^3/min and the total bed mass in the fuel reactor is $m_{tot} = 5$ kg. Moreover, κ can easily be calculated. Thus, to predict the conversion using Equation (11) and compare the result with experimental values during operation, the only missing parameter in the derivation above is k_F. Two methods for obtaining k_F are considered.

Method A utilizes experimental results from a lab unit operated with activated ilmenite and a bed mass $m_{tot} = 3$ or 6 g together with a fluidizing gas flow of $9\cdot10^{-4}$ Nm^3/min [25, 26]. In this study, syngas is added from below and there is no char gasification, *i.e.* $\kappa = 0$ and $p_g = 0$. Thus, Equation (7) reduces to (12):

$$dp = \frac{-k_F}{F_0}p\,dm \quad \text{or} \quad k_F = \frac{-F_0}{p}\frac{dp}{dm} \tag{12}$$

The solution to Equation (12) is:

$$p = p_0.e^{-\alpha} \tag{13}$$

using the same notations as above.

Finally the gas conversion reads:

$$\gamma_A = 1-e^{-\alpha} \tag{14}$$

Moreover, the relationship between the degree of conversion X of an oxygen carrier defined as:

$$X = \frac{m_{ox} - m}{m_{ox} - m_{red}} \tag{15}$$

and the degree of mass-based conversion ω is:

$$\omega = 1 - R_0 X \tag{16}$$

where R_0 is the actual oxygen transfer capacity of the oxygen carrier. Here, m_{ox} resp. m_{red} is the mass of a fully oxidized resp. reduced ilmenite particle.

This means that from experimental plots giving γ against ω, the syngas conversion can be read. In [20], it was shown from testing with activated ilmenite in the 10 kW_{th} unit that in order to satisfy both the heat and oxygen requirements in the fuel reactor, a maximum value for Δω of 2.1% is advisable. On the other hand, a lower value would correspond to an unnecessarily high particle circulation and thus a poorer CO_2 capture. Here, an interval of ω of 0.98-1 was used. Note that for values closest to 1, back-mixing considerably affects the results. To eliminate this effect, the cases where ω is above 0.995 are excluded from calculation with Method A. Then, extracting α from Equation (14) and introducing its value in (9), k_F can be deduced using the values for m_{tot} and F_0 for the lab unit. This k_F is now used in Equation (9) to calculate α for the 10 kW_{th} unit, and α is finally inserted in Equation (11) to obtain the conversion according to the model.

Method B utilizes the Shrinking Core Model (SCM) for the oxygen consumption within the ilmenite particles in combination with thermogravimetric analysis (TGA) results by Abad *et al*. (2010) [27]. The SCM has been used extensively in order to model reaction kinetics of different type of oxygen carrier particles with CH_4, CO and H_2, normally with chemical reaction control only. The kinetic equation for the shrinking-core model for spherical grain is:

$$\frac{t}{\tau_{comp}} = 1 - (1 - X)^{1/3} \tag{17}$$

where τ_{comp} is the time for complete conversion of the particle and calculated from:

$$\tau_{comp} = \frac{\rho_m r_g}{bkC^n} \tag{18}$$

Here, ρ_m is the molar density of the active solid phase, r_g the grain or particle radius, b the average stoichiometric coefficient for the reaction of solid with reacting gas and k the initial reaction rate constant. The unit for k is dependent upon the reaction order n, and is m/s for a first-order reaction [27]. C is the concentration of reactant and can be considered as a constant due to the excess of reactant in relation to the oxygen carrier inventory during experiment. In [27], ρ_m = 13.59 kmol/m^3, r_g = 125 μm and b = 1.45 for CO and H_2. Moreover, R_0 was here 3.3% for activated ilmenite.

The reaction rate constant k is a function of temperature and hence fitted to an Arrhenius-type equation:

$$k = k_0 e^{-E/RT} \tag{19}$$

From TGA experiment using syngas, the activation energy E and the pre-exponential factor k_0 can be obtained. Moreover, the reaction orders for H_2 and CO with activated ilmenite were determined to be 1 and 0.8 respectively [27].

An effective rate constant k_{eff} has been introduced in [28] as:

$$k_{eff} = -\frac{1}{p_m}\frac{d\omega}{dt} \tag{20}$$

where, p_m is a mean partial pressure of the reactant in the bed. Thus, inserting Equation (16) in Equation (17) and differentiating with respect to "t", and combining with Equation (20) gives:

$$k_{eff} = \frac{3R_0}{p_m \tau_{comp}} \cdot (1 - X)^{2/3} \tag{21}$$

Moreover, from a mass balance over a bed layer dm and using Equations (12) and (20), k_F and k_{eff} are related through Equation (22):

$$k_F = k_{eff} \cdot \frac{V_n p_{tot}}{f_{OF} M_O} \tag{22}$$

where V_n = 22.4 Nm^3/kmol, p_{tot} is the total pressure *i.e*. 1 bar, M_O is the molar mass of oxygen and f_{OF} is the stoichiometric ratio of oxygen consumed per mole of fuel oxidized, *i.e*. 1 for CO and H_2.

Finally, combining Equations (17, 20) and (21) gives:

$$k_F = \frac{3V_n p_{tot} R_0 b\, kC^n (1 - X)^{2/3}}{f_{OF} M_O \rho_m r_g p_m} \tag{23}$$

For a first order reaction, Equation (22) simplifies to:

$$k_F = \frac{3R_0 b\, k (1 - X)^{2/3}}{f_{OF} M_O \rho_m r_g} \cdot \frac{273}{273 + T} \tag{24}$$

Different values close to X = 0 can be chosen and the corresponding values of k_F can then be used in Equation (9) to calculate ω, which is subsequently used in Equation (11) to obtain the conversions.

4 RESULTS

4.1 Calculation of *kF*

As seen in Section 3, the mass-based rate constant k_F needs to be obtained first in order to determine the syngas conversions according to the model.

For *hydrogen* which exhibits a first order reaction with the ilmenite, methods A and B can be used directly.

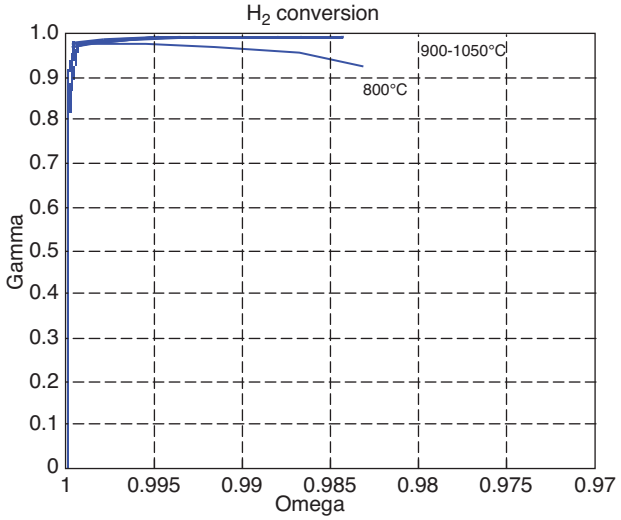

Figure 5

Hydrogen conversion γ_{H_2} (gamma) against degree of mass-based conversion ω (omega) for different temperatures. From [25].

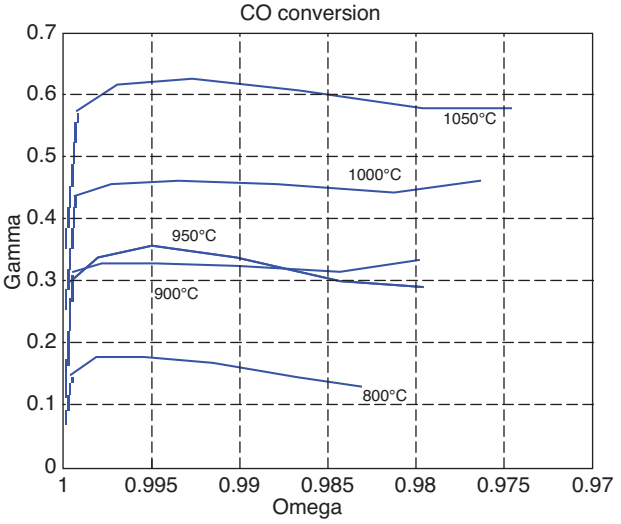

Figure 6

Carbon monoxide conversion γ_{CO} (gamma) against degree of mass-based conversion ω (omega) for different temperatures. From [25].

Method A: Unpublished results from Leion *et al*. (2010) provide the ilmenite conversions of H_2 at different temperatures and using a bed of 3 g ilmenite with a fluidizing flow of $9 \cdot 10^{-4}$ Nm^3/min [25], which means that $m/F_0 = 0.2$ ton·s/Nm^3. Figure 5 shows the results. Then, using these conversions in Equation (14), α can be extracted. From the definition of α in Equation (9) and with m/F_0 above, k_F is obtained in Nm^3/(ton.s), see Table 3.

For comparison, results from operation in the same laboratory unit but using 6 g of the activated ilmenite and a fluidizing syngas flow of $9 \cdot 10^{-4}$ Nm^3/min are also presented in Table 3. The values for hydrogen were taken from Figure 8 in [26]. Results differ with a factor 3, as virtually the same conversions are obtained for twice as large a bed inventory. It should be said that evaluation using method A gives significant uncertainty when conversions are very high as is the case for hydrogen. Nevertheless, the data give the order of magnitude and are useful for comparison to method B.

Method B: From results on H_2 conversion in TGA experiment, the pre-exponential factor and the activation energy in Equation (19) were determined [27]. Those were respectively $k_0 = 6.2 \cdot 10^{-2}$ m/s and $E = 65$ kJ/mol. This enables calculation of the kinetics constant k at each operating temperature, using Equation (19). Finally, Equation (24) gives the corresponding k_F.

There is a satisfying agreement in the results from methods A and B.

Note that a similar methodology is used in the calculation of k_F at each temperature and these results are shown in Section 4.2 below.

TABLE 3

kF (Nm^3/(ton.s)) for H_2 according to methods A and B at 950°C; A^1 using 3 g of ilmenite [25]; A^2 using 6 g of ilmenite [26]; B^3 using Equation (24); $R_0 = 3.3\%$ is used to convert X to ω

	$k_F(H_2)$		
Method	A^1 (3 g)	A^6 (6 g)	B^3
ω = 1 (X = 0)	-	-	12.2
ω = 0.995 (X = 0.15)	21.0	8.1	11
ω = 0.99 (X = 0.30)	23.0	8.8	9.6
ω = 0.985 (X = 0.45)	26.5	9.2	8.2
ω = 0.98 (X = 0.60)	31.1	9.2	6.6

For *carbon monoxide*, the order of reaction with activated ilmenite is 0.8, as obtained in [27].

For *method A*, a similar approach as above can be conducted, under the assumption of a first order reaction. Figure 6 shows the results from Leion *et al*. (2010) for the conversion against ω at different temperatures, using 3 g of ilmenite with a fluidizing flow of $9 \cdot 10^{-4}$ Nm^3/min [25].

The results for k_F are summarized in Table 4 for 950°C, and for both 3 and 6 g of ilmenite. In the case of 6 g of ilmenite, the values were taken from Figure 9 in [26]. Here, results for 3 and 6 g seem to agree reasonably well.

In *method B*, the pre-exponential factor and the activation energy in Equation (19) were determined to 0.1 $mol^{0.8}$ $m^{0.4}$ s^{-1} and 80.7 kJ/mol respectively [27].

To calculate k_F using Equation (23), a representative concentration $C_{CO} = p_{CO,m}/RT$ (in mol/m^3) must be chosen.

Note that reaction (23) transfers the reaction constant k, which has the reaction order 0.8, to a constant k_F assuming a first order reaction. Thus, k_F is somewhat dependent on $p_{CO,m}$ or C_{CO} and this should be considered when k_F is being used.

For operation with petroleum coke in the 10 kW$_{th}$ unit, $p_{CO,m}/p_{tot}$ = 0.02 is a fair approximation of the average carbon monoxide concentration in the bed of LOVEL [15-18]. In the laboratory unit, for an inlet CO concentration of 50% and a conversion of 35% at 950°C, $p_{CO,m}/p_{tot}$ = 0.4 can be chosen, see Figure 6 and [25].

Results from method B are summarized in Table 4, and k_F is calculated using Equation (23) for the two concentration cases above.

TABLE 4

k_F (Nm^3/(ton.s)) for CO according to methods A and B at 950°C; A[1] using 3 g of ilmenite [25]; A[2] using 6 g of ilmenite [26]; B[3] using Equation (23); R_0 = 3.3% is used to convert X to ω

Method	k_F (CO)			
	A[1] (3 g)	A[2] (6 g)	B[3] $p_{CO,m}/p_{tot}$ = 0.4	B[3] $p_{CO,m}/p_{tot}$ = 0.02
ω = 1 (X = 0)	-	-	3.2	5.8
ω = 0.995 (X = 0.15)	2.2	3.8	2.9	5.2
ω = 0.99 (X = 0.30)	2.15	3.4	2.5	4.6
ω = 0.985 (X = 0.45)	1.9	3.0	2.15	3.9
ω = 0.98 (X = 0.60)	2.1	2.8	1.7	3.2

As can be seen in Table 4, k_F derived at $p_{CO,m}/p_{tot}$ = 0.4 for method B agrees well with method A.

4.2 Syngas Conversion According to the Model

Here, conversion calculations are based on k_F obtained for ω = 0.99. Since only results at 950°C are available in [26], the values of k_F in method A will be calculated for the setup with 3 g ilmenite [25]. For the carbon monoxide, the values of k_F from method B will correspond to $p_{CO,m}/p_{tot}$ = 0.02.

From a series of tests using petroleum coke presented in [19], the results for experimental conversions of H_2 and CO in the 10 kW$_{th}$ unit could be obtained. For corresponding operation, κ was calculated to 0.017. Moreover, the ilmenite inventory was 5 kg and the steam fluidizing flow 3·10^{-2} Nm^3/min, which means that m/F_0 = 10 ton·s/Nm^3 [19].

Thus, the predicted conversion γ_{H_2} could be determined from Equation (11), see Table 5.

Table 5 indicates that the two methods give fairly similar conversion predictions. High predicted conversions according to the model are due to the high values for k_F and thus α, see Equation (11). This is consistent with the high hydrogen conversions obtained in the laboratory tests [25]. However, a large deviation between measured and predicted conversions can be noted.

TABLE 5

Comparison between experimental and predicted H_2 conversions at different temperatures. [a] Experimental conversions measured in the 10 kW$_{th}$ unit. [b] From Equation (11)

T (°C)	950	970	980	1000	1030	1050
10 kW$_{th}$ unit experiments						
γ_{H_2} [a] (%)	72	83	94.8	70.6	89.3	-
Method A						
kF	23.0					
γ_{H_2} [b] (%)	99.6					
Method B						
k_F	9.6	10.5	10.9	11.9	13.4	14.4
γ_{H_2} [b] (%)	98.9	99	99.1	99.1	99.2	99.3

The results for CO are summarized in Table 6.

TABLE 6

Comparison between experimental and predicted CO conversions at different temperatures. [a] Experimental conversions in the 10 kW$_{th}$ unit. [b] From Equation (11)

T (°C)	950	970	980	1000	1030	1050
10 kW$_{th}$ unit experiments						
γ_{CO} [a] (%)	91.6	89	95.2	89.2	90.1	-
Method A						
k_F	2.15	-	-	3.1	-	4.8
γ_{CO} [b] (%)	95.3	-	-	96.7	-	97.9
Method B						
k_F	4.6	5.1	5.4	6.1	7.1	7.8
γ_{CO} [b] (%)	97.8	98	98.1	98.3	98.6	98.8

For CO, the predicted conversions in Table 6 are somewhat higher for method B, which is because k_F becomes higher at lower values of $p_{CO,m}$. Again, the measured conversions are significantly lower than those predicted, although the difference is not as high as for hydrogen.

DISCUSSION

The conversion of the syngas from char gasification was modeled and results in Section 4.1 showed that there is a certain discrepancy with the experimental values obtained in the 10 kW$_{th}$ unit. Several factors that could explain this are discussed below.

Firstly, an important point in the comparison of the different methods is that the bed is fixed in the TGA experiment and the mass transfer is different compared to the laboratory fluidized beds. Moreover, the reactivity of the ilmenite can vary depending upon the activation procedure. This can well explain the variations in the determination of k_F seen in Tables 3 and 4. Nevertheless, the different approaches in determining k_F give consistent results and, independent from these variations in k_F, the model still predicts very much higher conversions than those actually measured.

Secondly, in the 10 kW_{th} unit, there was an excess of fluidizing steam and the water-gas shift:

$$CO + H_2O \rightarrow CO_2 + H_2 \quad (25)$$

was most likely pushed towards less CO and more H_2, as confirmed by the higher conversions of CO compared to H_2. As a consequence, the CO conversion agreed better with the higher model predictions. However, this shift from CO to H_2 does not explain the general difference in conversions between model and experiment.

Finally, recent results by Linderholm and Cuadrat (2010) [29] obtained in the same unit suggest that the volatiles released in the early phase following fuel introduction are prone to form soot. Thus, a possible explanation to the deviations could be that soot was deposited above the bed and was gasified, producing H_2 and CO. A related explanation is if there are char particles not fully mixed into the bed but located downstream the bed, e.g in the loop-seal below the fuel reactor cyclone.

CONCLUSIONS

Results from batch tests performed in a 10 kW_{th} CLC unit for solid fuels were used for comparison to model results. In these tests, ilmenite was the oxygen carrier and it was used in combination with two different fuels and different temperatures.

The idea with the present study was to obtain complementary information on the reactor system behavior. In previous work, it was possible to model the kinetics of the char conversion in the fuel reactor. Here, a model to predict the conversion of syngases CO and H_2 with ilmenite was derived. It involved either TGA or laboratory experiment for the calculation of rate constants for ilmenite. Results were compared with the actual conversions during operation in this 10 kW_{th} unit. There is a discrepancy between predicted and measured gas conversions. A possible explanation could be soot formation from the fuel volatiles.

ACKNOWLEDGMENTS

This work has been made with financial grant from the Research Fund for Coal and Steel of the European Community (Contract No: RFCP-CT-2008-00008).

REFERENCES

1 Cao Y. *et al*. (2005) Reduction of Solid Oxygen Carrier (CuO) by Solid Fuel (coal) in Chemical Looping Combustion, Preprints of Symposia - American Chemical Society, *Division of Fuel Chemistry* **50**, 1, 99-102.

2 Lyon R.K., Cole J.A. (2000) Unmixed Combustion: an Alternative to Fire, *Combust. Flame* **121**, 249-261.

3 Pan W.-P. *et al*. (2004) Application of a Circulating Fluidized-Bed Process for the Chemical Looping Combustion of Solid Fuels, Abstracts of Papers, *228th ACS National Meeting*, Philadelphia, PA, United States, August 22-26, p. 155.

4 Cao Y. *et al*. (2004) Application of a Circulating Fluidized-Bed Process for the Chemical Looping Combustion of Solid Fuels. Preprints of Symposia - American Chemical Society, *Division of Fuel Chemistry* **49**, 2, 815-816.

5 Mou J.-M., Xiang W.-G., Di T.-T. (2007) Performance Study of an Oxygen-Bearing Iron Oxide-Based Combined Cycle System featuring Integrated Coal Gasification Chemical Looping Combustion, *J. Eng. Thermal Energy Power* **22**, 2, 149-153.

6 Dennis J.S., Scott S.A., Hayhurst A.N. (2006) *In situ* Gasification of Coal using Steam with Chemical Looping: a Technique for Isolating CO_2 from Burning a Solid Fuel, *J. Energ. Institute* **79**, 187-190.

7 Scott S.A., Dennis J.S., Hayhurst A.N. (2006) *In situ* Gasification of Solid Fuel and CO_2 Separation using Chemical Looping, *AIChE J.* **52**, 9, 3325-3328.

8 Gao Z, Shen L., Xiao J., Qing C., Song Q. (2008) The use of Coal as Fuel for Chemical Looping Combustion with Ni-based Oxygen Carrier, *Ind. Eng. Chem. Res.* **47**, 23, 9279-9287.

9 Leion H., Mattisson T., Lyngfelt A. (2007) The Use of Petroleum Coke as Fuel in Chemical Looping Combustion, *Fuel* **86**, 1947-1958.

10 Leion H., Mattisson T., Lyngfelt A. (2008) Solid Fuels in Chemical Looping Combustion, *Int. J. Greenhouse Gas Control* **2**, 180-193.

11 Leion H., Lyngfelt A., Mattisson T. (2009) Solid Fuels in Chemical Looping Combustion using a NiO-based Oxygen Carrier, *Chem. Eng. Res. Des.* **87**, 1543-1550.

12 Leion H., Mattisson T., Lyngfelt A. (2008) CO_2 Capture from Direct Combustion of Solid Fuels with Chemical Looping Combustion, *Proceedings of the 33rd International Technical Conference on Coal Utilization & Fuel Systems*, Clearwater, FL, USA.

13 Leion H., Jerndal E., Steenari S., Hermansson M., Israelsson E., Jansson M., Johnsson M., Thunberg R., Vadenbo A., Mattisson T., Lyngfelt A. (2009) Solid Fuels in Chemical Looping Combustion using Oxide Scale and Unprocessed Iron Ore as Oxygen Carriers, *Fuel* **88**, 10, 1945-1954.

14 Shen L., Wu J., Xiao J. (2009) Experiments on Chemical Looping Combustion of Coal with a NiO based Oxygen Carrier, *Combust. Flame* **156**, 3, 721-728.

15 Berguerand N., Lyngfelt A. (2008) Design and Operation of a 10 kW_{th} Chemical Looping Combustor for Solid Fuels - Testing with South African Coal, *Fuel* **87**, 12, 2713-2726.

16 Berguerand N., Lyngfelt A. (2008) The Use of Petroleum Coke in a 10 kW_{th} Chemical Looping Combustor, *Int. J. Greenhouse Gas Control* **2**, 2, 169-179.

17 Berguerand N., Lyngfelt A. (2009) Operation in a 10 kW_{th} Chemical Looping Combustor for Solid Fuel - Testing with a Mexican Petroleum Coke, *Energy Procedia* **1**, 407-414.

18 Berguerand N., Lyngfelt A. (2009) Chemical Looping Combustion of Petroleum Coke using Ilmenite in a 10 kW$_{th}$ unit - High Temperature Operation, *Energ. Fuel.* **23**, 10, 5257-5268.

19 Berguerand N., Lyngfelt A. (2010) Batch Testing of Solid Fuels with Ilmenite in a 10 kW$_{th}$ Chemical Looping Combustor, *Fuel* 89, 1749-1762.

20 Markström P., Berguerand N., Lyngfelt A. (2010) The Application of a Multistage-Bed Model for Residence-Time Analysis in Chemical Looping Combustion of Solid Fuel, *Chem. Eng. Sci.* **65**, 5055-5066.

21 Shen L., Wu J., Xiao J. (2009) Experiments on Chemical Looping Combustion of Coal with a NiO based Oxygen Carrier, *Combust. Flame* **156**, 3, 721-728.

22 Wu J., Shen L., Hao J., Gu H. (2010) Chemical Looping Combustion of Coal in a 1 kW$_{th}$ reactor with Iron Ore as an Oxygen Carrier, Unpublished results.

23 Cuadrat A., Abad A., Adanez J., de Diego L., Garcia-Labiano F., Gayan P. (2009) Behaviour of Ilmenite as Oxygen Carrier in Chemical Looping Combustion, in *Clean Coal Technology Conference*, Dresden.

24 Adanez J., Cuadrat A., Abad A., Gayan P., de Diego L.-F., Garcia-Labiano F. (2010) Ilmenite Activation during Consecutive Redox Cycles in Chemical Looping Combustion, *Energ. Fuel.* **24**, 2, 1402-1413.

25 Leion H. *et al.* (2010) Unpublished results.

26 Azis M., Jerndal E., Leion H., Mattisson T., Lyngfelt A. (2010) On Evaluation of Synthetic and Natural Ilmenite using Syngas as Fuel in Chemical Looping Combustion (CLC), *Chem. Eng. Res. Des.*, in press.

27 Abad A., Adanez J., Cuadrat A., Garcia-Labiano F., Gayan P., de Diego Luis F. (2010) *Kinetics of Redox Reactions of Ilmenite for Chemical Looping Combustion*, Submitted for publication.

28 Johansson M. (2007) Screening of Oxygen Carrier Particles based on Iron-, Manganese-, Copper-, and Nickel Oxides for Use in Chemical Looping Technologies, *PhD Thesis*, Environmental Inorganic Chemistry, Chalmers University of Technology, Göteborg.

29 Linderholm C., Cuadrat A. (2010) Unpublished results.

Final manuscript received in September 2010
Published online in February 2011